

# Silica-Supported Tungsten Neosilyl Oxo Precatalysts: Impact of the Podality on Activity and Stability in Olefin Metathesis

D. Grekov,<sup>‡</sup> Y. Bouhoute,<sup>†</sup> K. C. Szeto,<sup>†</sup> N. Merle,<sup>†</sup> A. De Mallmann,<sup>†</sup> F. Lefebvre,<sup>†</sup> C. Lucas,<sup>†</sup> I. Del Rosal,<sup>§</sup> L. Maron,<sup>\*,§</sup> R. M. Gauvin,<sup>‡</sup> L. Delevoye,<sup>\*,‡</sup> and M. Taoufik<sup>\*,†</sup>

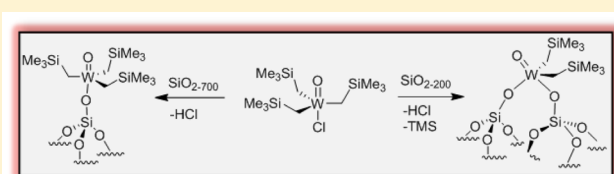
<sup>†</sup>Laboratoire de Chimie, Catalyse, Polymères et Procédés, UMR 5265 CNRS/ESCPE-Lyon/UCBL, ESCPE Lyon, F-308-43, Boulevard du 11 Novembre 1918, F-69616 Villeurbanne Cedex, France

<sup>‡</sup>Univ. Lille, CNRS, Centrale Lille, ENSCL, Univ. Artois, UMR 8181 - UCCS - Unité de Catalyse et Chimie du Solide, F-59000 Lille, France

<sup>§</sup>Laboratoire de Physico-Chimie des Nano-Objets, CNRS UMR 5215, Université de Toulouse, INSA, UPS, 135 Avenue de Rangueil, F-31077 Toulouse, France

## Supporting Information

**ABSTRACT:** In order to establish structure–reactivity relationships in propylene metathesis as a function of the podality of tungsten oxo species bearing neosilyl ligands, we targeted the parent tris alkyl [(≡SiO)WOR<sub>3</sub>] and bis alkyl oxo [(≡SiO)<sub>2</sub>WOR<sub>2</sub>] derivatives prone to carbene formation. Thus, [WO(CH<sub>2</sub>SiMe<sub>3</sub>)<sub>3</sub>Cl] (1) was grafted onto silica dehydroxylated at 700 °C (SiO<sub>2-700</sub>), proceeding via W–Cl cleavage to yield well-defined monopodal species [(≡SiO)-WO(CH<sub>2</sub>SiMe<sub>3</sub>)<sub>3</sub>] (2a) along with HCl release. On the other hand, the corresponding bipodal species [(≡SiO)<sub>2</sub>WO(CH<sub>2</sub>SiMe<sub>3</sub>)<sub>2</sub>] (2b) was obtained on SiO<sub>2-200</sub> by release of both HCl and TMS. The formation of these species were demonstrated by mass balance analysis, elemental analysis, IR, advanced solid-state NMR (1D and 2D <sup>1</sup>H, <sup>13</sup>C, <sup>29</sup>Si, and <sup>17</sup>O), and EXAFS. Furthermore, DFT calculations allowed understanding and rationalizing the experimental results regarding grafting selectivity. Materials 2a and 2b proved to lead to stable and efficient supported tungsten oxo catalysts for propene metathesis under dynamic conditions at 80 °C. The symmetric bipodal precatalyst (expressed as [W(=E)(=CHR)(X)(Y)] (X = Y, E = spectator ligand)) showed somewhat higher activity than the asymmetric (X ≠ Y) counterparts.



## Highly active Olefin Metathesis Catalysts

## INTRODUCTION

Tungsten oxide supported on silica is an efficient catalyst for olefin metathesis used in industrial processes since the 1960s on a large-scale in Phillips' neohexene process and ABB Lummus' olefins conversion technology (OCT).<sup>1</sup> This heterogeneous catalyst is classically prepared by incipient wetness impregnation of ammonium metatungstate followed by calcination.<sup>2</sup> Different surface species, difficult to distinguish, are inevitably generated upon the calcination step despite modification of the preparation procedure.<sup>3–8</sup> The nature of the active site still needs to be determined, but WO<sub>3</sub> crystallites can be excluded as an active species.<sup>1,9</sup> The catalytic activity is attributed to a bipodal isolated tungsten(VI) center bearing an oxo ligand and carbene fragment.<sup>10,11</sup> Such a surface species exists only in very low concentration in the commercialized catalyst. Other tungsten species are formed during catalyst preparation and pretreatment in the presence of water, which can enhance the mobility of WO<sub>3</sub> on the silica support and result in poor dispersion. In order to avoid water in the preparation steps, we have developed an anhydrous route for the preparation of supported tungsten oxo metathesis (pre)-catalysts by surface organometallic chemistry. The very first

well-defined silica-supported tungsten oxo species active in olefin metathesis was prepared by grafting of [O=W-(CH<sub>2</sub>tBu)<sub>4</sub>] or [O=WCl(CH<sub>2</sub>tBu)<sub>3</sub>] complexes, both affording tungsten oxo tris-neopenyl surface species grafted on silica through a single W–O–Si bond.<sup>12,13</sup> As expected, this material catalyzes propylene self-metathesis after *in situ* generation of the tungsten carbene moiety at 80 °C. The striking discovery was that this catalyst showed an enhanced stability with time on stream compared to the corresponding imido-supported catalyst, which deactivated rapidly by reduction of the metal through decomposition of the metallacyclobutane intermediate.<sup>12</sup> Our findings were later on confirmed by other research groups from a theoretical approach.<sup>14</sup> Inspired by these pioneering works, notably on supported tungsten oxo catalysts, other groups have newly turned their interest to monopodal tungsten oxo species on amorphous silica.<sup>15,16</sup> So far, it was well accepted that the proposed active center of the industrial WO<sub>3</sub>/SiO<sub>2</sub> catalyst is isolated bipodal tungsten oxo species. Recently, it has been

Received: March 18, 2016

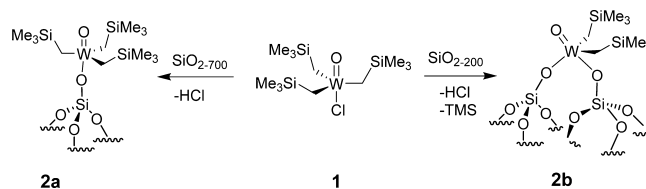
proposed for the isoelectronic  $\text{MoO}_3/\text{SiO}_2$  olefin metathesis catalyst that the active site may also be a monopodal species, which can more easily lead to the active carbene by assistance of the acidic Mo-OH proton.<sup>17</sup> This stirs up the debate about the nature of the active site in supported group VI metathesis catalysts. It is evident that the podality will directly affect the electrophilicity and rigidity/flexibility around the metal center that may have an impact on the catalytic activity. Moreover, DFT calculations have investigated the effect of the spectator ligands X and Y (when expressing the active site as  $[\text{M}(=\text{E})(=\text{CHR})(\text{X})(\text{Y})]$  ( $\text{M} = \text{Mo}, \text{W}$ ;  $\text{E} = \text{oxo}, \text{imido}$ ) and predicted that high-performance catalysts should contain both good (X, for example, alkyl) and poor (Y, for example, siloxy)  $\sigma$ -donor ligands.<sup>18</sup> Prior to elucidating all these effects, it is necessary to develop well-defined supported species exhibiting different coordination spheres mentioned above. Monopodal tungsten species can easily be obtained by room-temperature grafting of a suitable organometallic complex on silica dehydroxylated at 700 °C by protonolysis of the W-C, W-Cl, W-N, or W-OR bond.<sup>12,13,16,19</sup> However, to design a silica-supported bipodal tungsten oxo species is a far more complex task. Grafting of  $\text{WONp}_3\text{Cl}$  on silica dehydroxylated at 200 °C (a support that frequently affords bipodal species<sup>20–22</sup>) led only to silica-supported monopodal tungsten oxo neopentyl species by selective protonolysis of the W-Cl bond.<sup>23</sup> Further heat treatment of the latter material to initiate the formation of bipodal species  $[(\equiv\text{SiO})_2\text{WO}(\text{CH}_2t\text{Bu})_2]$  via W-C cleavage by a neighboring SiOH was unsuccessful. In the quest for a realistic model of the active species within the key industrial catalyst  $\text{WO}_3/\text{SiO}_2$ , we have recently succeeded in preparing an oxo-bis-alkyl tungsten complex doubly anchored on the silica support. This was accomplished by a switch from neopentyl to neosilyl group, which facilitates the W-C activation, thus enabling formation of the targeted bipodal structure through consecutive W-Cl and W-C silanolysis on a mildly dehydroxylated  $\text{SiO}_{2-200}$  support.<sup>23</sup> This material efficiently performs propene metathesis under relatively mild conditions (80 °C), with sustained activity, in contrast to other recently reported monopodal tungsten oxo species bearing bulky aryloxy ligands that rapidly deactivate under the given conditions.<sup>16</sup>

Although these recently published results indicate that there is a notable difference in the catalytic performance between the supported bipodal and monopodal tungsten oxo catalysts, up to now, no direct comparison has been made on the metathesis activity of monopodal and bipodal tungsten oxo species issued from the same molecular precursor. Thus, this work is aiming at the systematic investigation of structure–reactivity relationships in propene metathesis as a function of the podality of tungsten oxo species bearing neosilyl ligands. Simultaneously, other related supported tungsten oxo species substituted with different spectator ligands have been studied in order to determine the effect of the  $\sigma$ -donor spectator ligands (that is, neosilyl vs neopentyl, siloxide or aryloxy) and thus to further contribute to the building of structure–activity relationships.

## RESULTS AND DISCUSSION

The grafting of  $[\text{O}=\text{WCl}(\text{CH}_2\text{SiMe}_3)_3]$  (**1**) on silica dehydroxylated at 700 °C was carried out under dynamic vacuum in order to continuously remove HCl that is released upon reaction with silanols and thus to shift the equilibrium toward formation of surface species **2a** (Scheme 1). This affords a white powder, whereas, for comparison, grafting of **1**

### Scheme 1. Reaction of **1** with $\text{SiO}_{2-700}$ and $\text{SiO}_{2-200}$



on  $\text{SiO}_{2-200}$  produces a yellow material. Infrared studies show depletion of the isolated silanols at  $3747\text{ cm}^{-1}$  (Figure 1).

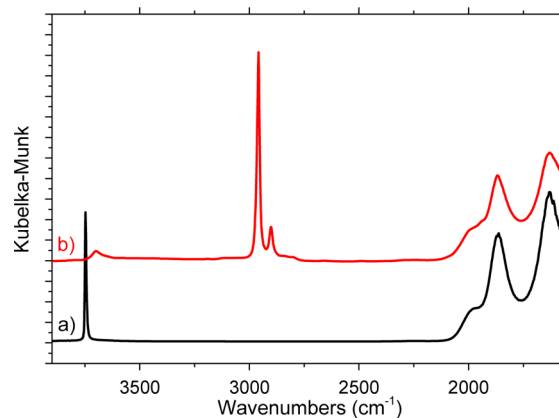


**Figure 1.** DRIFT spectra of  $\text{SiO}_{2-700}$  (a) and after reaction with  $[\text{O}=\text{WCl}(\text{CH}_2\text{SiMe}_3)_3]$ , **2a** (b).

Furthermore, new peaks corresponding to  $\nu(\text{C-H})$  and  $\delta(\text{C-H})$  of alkyl fragments also appeared. Elemental analysis of this material indicates a W and C percent content of 4.54%<sub>wt</sub> and 3.42%<sub>wt</sub>, respectively, which corresponds to a C/W molar ratio of 11.5 (theoretical for **2a**: 12). Furthermore, gas phase analysis reveals that the only product released is HCl ( $220\text{ }\mu\text{mol}\cdot\text{g}(\text{SiO}_{2-700})^{-1}$ , quantified by IR spectroscopy). In addition, the  $^1\text{H}$  MAS and  $^{13}\text{C}$  CP MAS NMR data show the presence of tungsten methylenic fragments, as reflected by the  $^1\text{H}$  and  $^{13}\text{C}$  signals at 1.3 and 66 ppm, respectively (Figure 2). The  $^{29}\text{Si}$  CP MAS NMR spectrum exhibits two signals at 1.2 and  $-100$  ppm, accounting for the neosilyl fragment and the silica support,<sup>24</sup> respectively (Figure 3). From these combined spectroscopic and analytical elements, it can be concluded that the reaction of

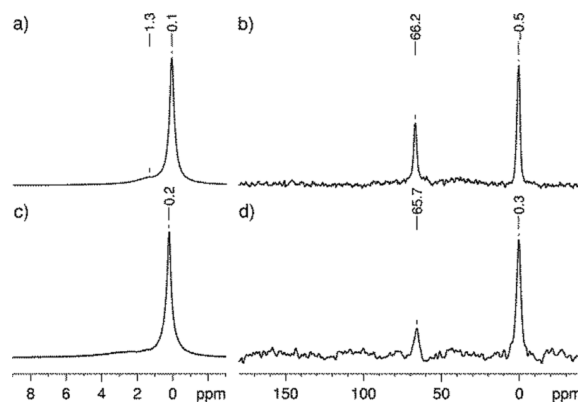


**Figure 2.** NMR characterization:  $^1\text{H}$  MAS NMR spectra of **2a** (a) and **2b** (c) and  $^{13}\text{C}$  CPMAS NMR spectra of **2a** (b) and **2b** (d) (11.75 T, spinning rate 10 kHz).

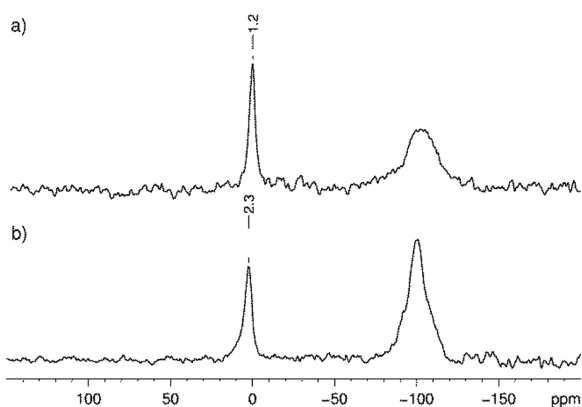


**Figure 3.**  $^{29}\text{Si}$  CP MAS NMR spectra of **2a** (a) and **2b** (b) (11.75 T, spinning rate 5 kHz).

**1** with the silica surface dehydroxylated at 700 °C proceeds by W–Cl silanolysis with concomitant HCl release, leading to a monopodal surface species,  $[(\equiv\text{SiO})\text{WO}(\text{CH}_2\text{SiMe}_3)_3]$  (**2a**) (Scheme 1).

The solid-state NMR data ( $^1\text{H}$ ,  $^{13}\text{C}$ ,  $^{29}\text{Si}$ ) of **2a** feature the expected signals of an anchored tungsten oxo neosilyl species. The relative peak intensity between **2a** and **2b** may indicate the number of neosilyl ligands and the nature of the grafted species. Noteworthy, the  $\text{WCH}_2$  signal intensity in **2a** in the  $^{13}\text{C}$  CPMAS spectrum is higher than that of **2b**, in line with the presence of three neosilyl ligands in **2a** compared to two neosilyl moieties in **2b**. A similar phenomenon is also observed in the  $^{29}\text{Si}$  CPMAS NMR spectrum, as the signal from the neosilyl ligand (1.2 ppm) in **2a** is more intense than that of **2b**. There is furthermore a difference in relative intensity of the silica-support peak at  $-100$  ppm,<sup>24</sup> consistent with the higher abundance of residual silanol groups in **2b** than in **2a**, as observed by infrared spectroscopy.

The former findings were further confirmed by an XAS study at the W  $L_{\text{III}}$  edge. EXAFS spectra of both the molecular complex **1** and the supported species **2a** were recorded in order to determine and compare the structures of the tungsten complexes.

The EXAFS spectrum for **1** has been recently published,<sup>23</sup> and the results are consistent with the following coordination sphere around W: one oxygen atom at 1.694(8) Å, assigned to

an oxo ligand, ca. three carbons at 2.10(1) Å, and one chloride at 2.41(1) Å. The observed distances are within the same range as reported for complexes with similar coordination spheres.<sup>25–29</sup>

For **2a** (grafting of **1** onto  $\text{SiO}_{2-700}$ ) the almost complete disappearance of the direct W–Cl and multiple (O=W–Cl) scattering pathways is clearly observed (Figure 4) when comparing the moduli of the Fourier transforms of both molecular and supported species. The contribution of the Cl backscatterer at ca. 2.1 Å and of the multiple scattering pathways at ca. 3.7 Å with no phase correction is observed on the Fourier transform corresponding to the molecular complex **1** (Figure 4). The values extracted from the fit of the EXAFS spectrum (Table 1) agree with one oxo ligand at 1.702(6) Å,

**Table 1.** EXAFS Parameters for the Supported Complex **2a**<sup>a</sup>

type of neighbor	number of neighbors	distance (Å)	$\sigma^2$ (Å <sup>2</sup> )
W=O	1.0(1)	1.702(6)	0.0007(5)
W–OSi≡	1.1(2)	1.93(2)	0.0050(23)
W–CH <sub>2</sub> SiMe <sub>3</sub>	2.9(3) <sup>b</sup>	2.09(1)	0.0026(9)
WCH <sub>2</sub> SiMe <sub>3</sub>	2.9 <sup>b</sup>	3.44(3)	0.0025(15)
W–OSi≡ <sup>c</sup>	1.1 <sup>b</sup>	3.51(3)	0.006(4)

<sup>a</sup>The errors generated by the EXAFS fitting program “RoundMid-night” are indicated in parentheses.  $\Delta k$ : [1.9–17.7 Å<sup>-1</sup>] –  $\Delta R$ : [0.7–3.6 Å] ([0.7–2.3 Å], when considering only the first coordination sphere);  $S_0^2 = 0.94$ ;  $\Delta E_0 = 6.5 \pm 1.0$  eV (the same for all shells); fit residue:  $\rho = 5.0\%$ ; quality factor:  $(\Delta\chi)^2/\nu = 1.97$ , with  $\nu = 16/31$  ( $[(\Delta\chi)^2/\nu]_1 = 2.50$  with  $\nu = 9/18$ , considering only the first coordination sphere: =O, –O, and –C). <sup>b</sup>Shell constrained to the parameters above. <sup>c</sup>Two (W–O–Si) types of multiple scattering pathways (3 and 4 legs,  $R = 3.55(5)$  Å and  $\sigma^2 = 0.0025(15)$  Å<sup>2</sup>) have also been considered in the fit but not mentioned in this table.

along with ca. one oxygen at 1.93(2) Å and ca. three carbon atoms at 2.09(1) Å, respectively assigned to one siloxide and three neosilyl ligands. The W–OSi≡ and W–C bond distances are in the same range as those observed in the  $\text{Me}_3\text{SiO–W}(\text{Ns})_3\text{O}$  moieties of the bimetallic complexes  $[\text{Me}_3\text{SiO–W}(\text{CH}_2\text{SiMe}_3)_3\text{O–W}(\text{CH}_2\text{SiMe}_3)_3(\equiv\text{C–SiMe}_3)]$  (2.084 to 2.104 Å for W–C and 1.906 to 1.930 Å for W–OSiMe<sub>3</sub>),<sup>28</sup> while the W=O bond distance found here for the supported complex is slightly shorter than that observed for these moieties (1.729–1.746 Å), where the oxo ligand also

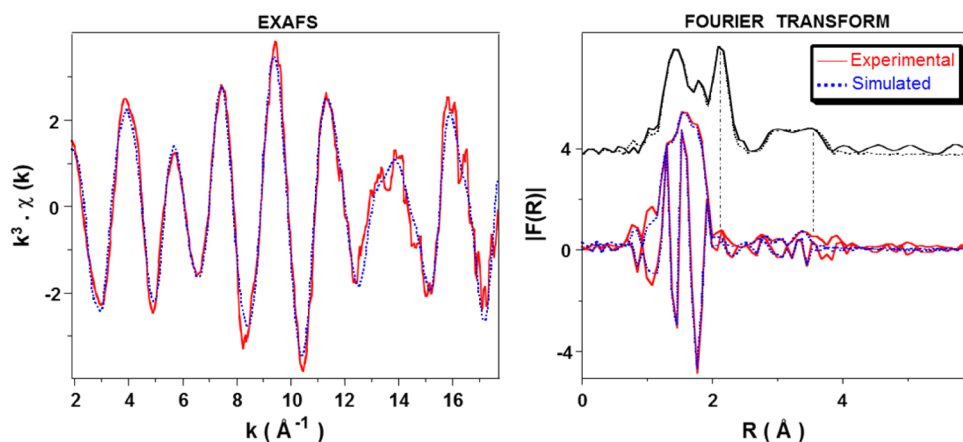


**Figure 4.** Tungsten  $L_{\text{III}}$ -edge  $k^3$ -weighted EXAFS (left) for **2a** and corresponding Fourier transform (right; modulus and imaginary part). In black: Fourier transform corresponding to the molecular complex **1** for comparison, superimposed with simulated curve. Solid lines: experimental; dashed lines: spherical wave theory.

interacts with another neighboring tungsten ( $W=O\cdots W$  at 2.578(6) Å). The  $W=O$  bond distance observed for **2a** is, however, typically in the range found for similar complexes, as for  $[O(WO(CH_2CMe_3)_2)_2]$ ,<sup>25</sup> with  $W=O$  in the range 1.676–1.736 Å ( $W-C$ : 2.113 to 2.150 Å) or for  $[OWCp(CH_2SiMe_3)_3]$ ,<sup>26</sup> with 1.664(8) Å for  $W=O$  ( $W-C$  of the neosilyl ligands: 2.231 to 2.322 Å). The relatively long  $W-O$  bond distance observed for  $\equiv SiO-W$  may indicate that the oxo and the siloxy ligand are located *trans* to each other in **2a**, as expected for a trigonal bipyramidal geometry, as observed for the  $Me_3SiO-W(=O)(CH_2SiMe_3)_3$  moieties of the bimetallic complex  $[Me_3SiOW(CH_2SiMe_3)_3O-W(CH_2SiMe_3)(\equiv C-SiMe_3)]$  or for the silica-supported complex  $[\equiv SiOW(O)(CH_2CMe_3)_3]$ .<sup>12,13</sup> Similar parameters were obtained when fitting the  $k^2\chi(k)$  spectrum. The fit could also be improved by adding two layers of silicon backscatterers, one composed of ca. three silicon atoms at 3.44(3) Å, attributed to the silicon of the neosilyl ligands, and another one with ca. one silicon atom at 3.51(3) Å, assigned to a silicon atom of a surface siloxide ligand. The shorter  $W-Si$  distance corresponds indeed to the distances of 3.417 to 3.448 Å found in the case of Si atoms of the neosilyl ligands within the bimetallic complex  $[Me_3SiO-W(CH_2SiMe_3)_3O-W(CH_2SiMe_3)_3(\equiv C-SiMe_3)]$  already mentioned above,<sup>28</sup> where  $[W-C-Si]$  angles from 118.9(2)° to 119.1(3)° were found.

In comparison, for the supported bipodal complex on  $SiO_{2-200}$ ,  $[(\equiv SiO)_2WO(CH_2SiMe_3)_2]$  (**2b**), shorter  $W-O$  distances were found for the two  $\equiv SiO-W$  bonds in **2b** (1.86(1) Å) than that obtained for **2a**  $[(\equiv SiO)WO(CH_2SiMe_3)_3]$  (1.93(2) Å) and for  $[(\equiv SiO)WO(CH_2tBu)_3]$  (1.98(2) Å).<sup>16</sup> This may indicate that the oxo and a siloxy ligand are not *trans* to each other in this bipodal surface complex.

The grafting reaction of complex **1** onto silica dehydroxylated at 700 °C ( $SiO_{2-700}$ ) was investigated computationally using DFT theory in order to gain further insights on the above-described experimental data. In the present study, we apply as surface model a cage-like polyoligosilsesquioxane derivative called *c* model (Figure S1). The two upper silicon atoms, linked through a siloxane bridge, reproduce the emerged part of the silica surface, i.e., an isolated silanol group for a silica dehydroxylated at 700 °C. This layer is surrounded by a layer built around four silicon atoms themselves surrounded by another layer formed by two silicon atoms added in order to increase the rigidity of the model. Both silicon atoms are connected to hydroxyl groups in order to saturate the model. In the same way,  $SiH_3$  groups are added, on the emerged part of the silica, to saturate the lateral siloxane bridges formed during the dehydroxylation reaction of the silica surface. This model has been found to be useful to confirm and further refine the understanding of the grafting reaction of several organometallic complexes onto silica dehydroxylated at 700 °C.<sup>13,23,30–35</sup>

The Gibbs free energy reaction profile for the grafting reaction of complex **1** onto  $SiO_{2-700}$  *c* model is depicted in Figure 5. The key geometrical parameters of the different stationary points are gathered in Table S1 in the Supporting Information. To shed light on the grafting reaction of complex **1** onto *c* model, as earlier studied for the grafting reaction of an oxo tris-neopentyl chloride system onto the same model,<sup>13</sup> the  $W-Cl$  silanolysis (with the concomitant HCl release) and the  $W-Ns$  cleavage (leading to the production of free tetramethylsilane, TMS) have been considered. In this case, as for the neopentyl system, the  $W-Cl$  silanolysis is kinetically

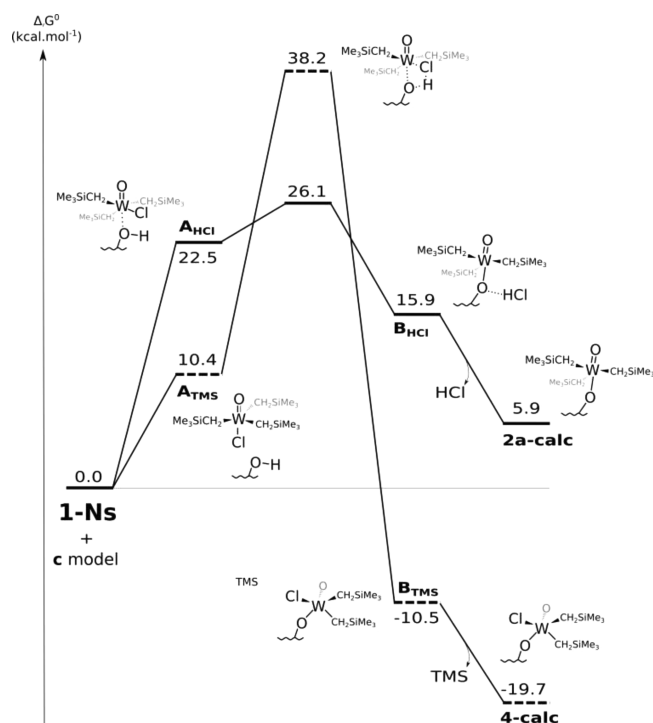


Figure 5. Gibbs Free Energy Profile for the Grafting Reaction of **1** onto *c* Model.

more favorable than the  $W-Ns$  cleavage. However, the  $W-Ns$  cleavage leads to the most stable product, i.e., the thermodynamic product. In both cases, an energetically costly Berry pseudorotation of **1** is necessary in order to allow the formation of an interaction between the metal center and the silanol group of *c* model. However, it is noteworthy that the transition states of the  $W-Ns$  silanolysis are around 12 kcal  $mol^{-1}$  higher than for those of the  $W-Cl$  silanolysis. This difference can be explained by the electrostatic effects since the greater steric hindrance around the metal center in  $TS(A_{TMS} \rightarrow B_{TMS})$  (Figure 6b) than in  $TS(A_{HCl} \rightarrow B_{HCl})$  (Figure 6a)

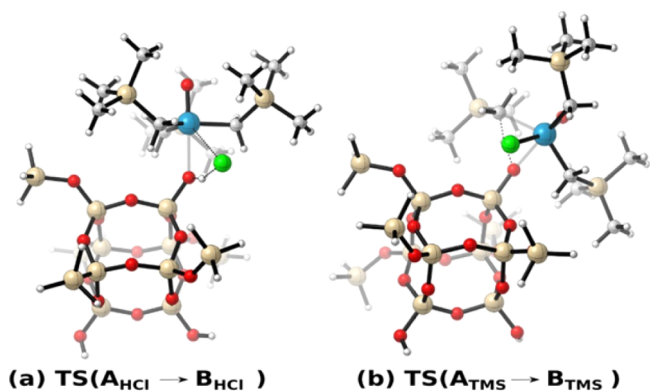
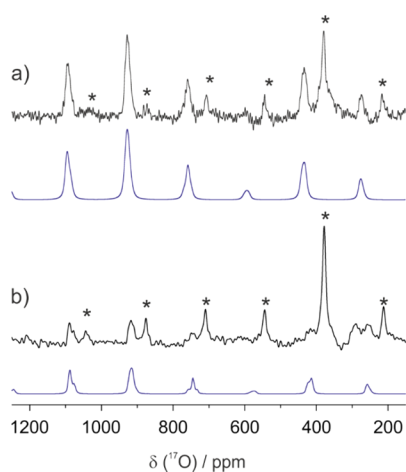


Figure 6. Optimized structures of the transition states in the grafting reaction of **1** onto *c* model.

destabilizes the system due to the electrostatic repulsion between the silica surface and the neosilyl ligands. This difference confirms the observed  $W-Cl$  cleavage process, affording  $[\equiv SiOWONs_3]$  surface species, and ruled out the  $W-Ns$  silanolysis grafting pathway.

From a thermodynamic point of view, the formation of monografted tungsten oxo tris-neosilyl complex **2a-calc** (Figure S2c) is a slightly endergonic process (+5.9 kcal mol<sup>-1</sup> with respect to the separated reactants), which is consistent with the fact that the experiment should be performed under dynamic vacuum in order for the reaction to proceed toward formation of **2a-calc**. In **2a-calc**, as suggested by <sup>17</sup>O NMR spectroscopic data (see below), the tungsten atom adopts a slightly distorted trigonal bipyramidal geometry with the three neosilyl ligands in equatorial sites ( $\text{W}-\text{CH}_2\text{SiMe}$  distances around 2.103 Å) and the oxo and the oxygen atom of the silica surface occupying the two axial sites ( $\text{W}=\text{O}$  and  $\text{W}-\text{OSi}\equiv$  distances of 1.712 and 1.995 Å, respectively).

We have previously demonstrated that <sup>17</sup>O solid-state NMR spectroscopy is a most efficient tool for the advanced characterization of molecular and supported catalysts.<sup>13,23,30,35</sup> Most particularly, the metal oxo moiety affords highly informative spectroscopic data that, when combined with DFT calculations, can allow access to molecular-level structural information. Thus, the isotopically enriched supported species **2a\*** was prepared by grafting the <sup>17</sup>O-enriched chloro trisalkyl species **1\*** (featuring a <sup>17</sup>O-labeled oxo moiety) onto the SiO<sub>2-700</sub> support.<sup>23</sup> The <sup>17</sup>O MAS NMR spectrum of **2a\*** is displayed in Figure 7a. As previously reported in related cases, a



**Figure 7.** <sup>17</sup>O MAS NMR spectra and corresponding best fit simulations of (a) **2a\*** (21.15 T, spinning speed 20 kHz) and (b) **2b\*** (18.8 T, spinning speed 18 kHz). Asterisks designate the rotor's ZrO<sub>2</sub> signal.

line shape characteristic of both significant chemical shift anisotropy and quadrupolar coupling is observed. Due to the lack of discontinuity within the resonances, precise assessment of the NMR parameters remains uncertain. From a best fit simulation, we propose a chemical shift of 774 ppm (±2), along with chemical shift anisotropy of -1110 ppm (±30) and a quadrupolar coupling constant of 5.2 MHz (±0.2). This compares rather well with DFT-calculated values on a model species (Figure S2c) respectively of 760 ppm, -1155 ppm, and 5.7 MHz, thus confirming the molecular structure of the surface species. For comparison, the <sup>17</sup>O NMR spectrum of **2b\*** is given in Figure 7b. The signal-to-noise ratio of the spectrum of **2b\*** does not allow determining precisely the NMR parameters for comparison to that of **2a\***. The isotropic chemical shift (which is unambiguously determined) is marginally affected by the structural changes between the two species, as it differs by 8 ppm only (766 ppm for **2a\***). We are facing the limits of <sup>17</sup>O NMR as applied to this series of grafted species, as mentioned in our previous studies.<sup>23</sup>

Academic and industrial scientists are pursuing the search of highly active and stable metathesis catalysts. Insights into the structure–reactivity relationships by determining the role of the podality and of the ancillary ligands (oxo, imido, aryloxo, pyrrolidyl, alkyl, siloxide) are keys to design active and stable metathesis catalysts.<sup>36</sup> However, there are several reports in the literature that rely mostly on the initial turnover frequency (TOF) for selected substrates and sometimes on the time to reach the thermodynamic equilibrium in the batch reactor in order to determine the activity of the catalyst.<sup>16,18,37</sup> These data reflect the initial activity of the catalyst, but give no information about the robustness and the productivity in the long run, which are critical parameters for potential industrial use. Moreover, in these studies, some examples display a very high initial activity, while undergoing rapid deactivation. Hence, it is not sufficient to compare the catalytic performance of different catalysts based only on the initial TOF.<sup>18</sup> A more rigorous, general method to probe the activity and stability of such catalysts is to perform continuous flow studies, in which the substrate to catalyst ratio is very high. This allows assessment of the cumulated turnover number (TON) after a given time. This approach is also closer to classical industrial preferences, i.e., the productivity after a defined time frame.

We first studied the catalytic performances of the monopodal species **2a** in a flow reactor (20 mL<sub>C<sub>3</sub>H<sub>6</sub></sub> min<sup>-1</sup>; 60 mol<sub>C<sub>3</sub>H<sub>6</sub></sub> mol<sub>W</sub><sup>-1</sup> min<sup>-1</sup>, 80 °C). The conversion profile (Figure 8) is described by a longer induction period with respect to **2b** (of

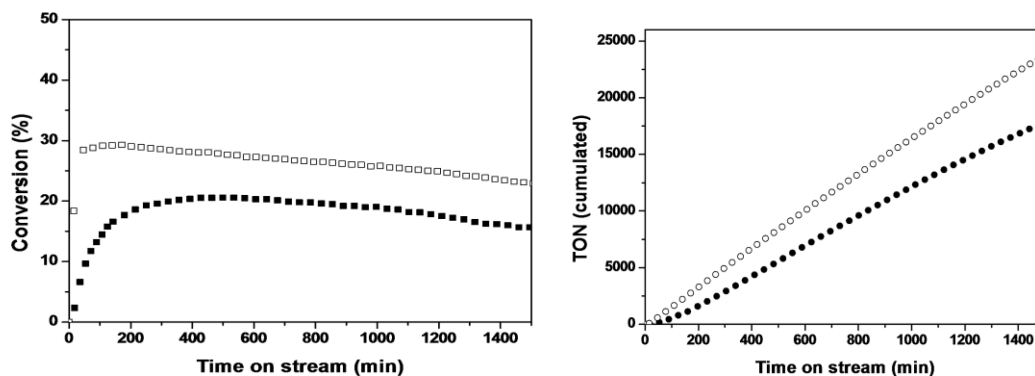


**Figure 8.** Conversion (left) and cumulated TON (right) of propylene self-metathesis (20 mL<sub>C<sub>3</sub>H<sub>6</sub></sub> min<sup>-1</sup>; 80 °C; 60 mol<sub>C<sub>3</sub>H<sub>6</sub></sub> mol<sub>W</sub><sup>-1</sup> min<sup>-1</sup>, 1 bar) over **2a** (■) and **2b** (□).

**Table 2. Comparative Propylene Metathesis Results for the Tungsten Oxo Catalysts: Activity (Cumulated TON) and Product Selectivity after 25 h of Reaction in a Dynamic Flow Reactor**

precatalyst	TOF <sup>a</sup>	TON <sup>b</sup>	product selectivity [%] <sup>c</sup>			
	(at 60 min)	(after 25 h)	ethylene	<i>E</i> -2-butene	<i>Z</i> -2-butene	<i>Z/E</i>
$[(\equiv\text{SiO})\text{WO}(\text{CH}_2\text{SiMe}_3)_3]$ , <b>2a</b>	3.3	18 000	50.0	31.0	19.0	0.61
$[(\equiv\text{SiO})_2\text{WO}(\text{CH}_2\text{SiMe}_3)_2]$ , <b>2b</b>	14.1	24 000	50.0	33.8	16.2	0.48
$[(\equiv\text{SiO})\text{WO}(\text{CH}_2\text{CMe}_3)_3]$ , <b>2c</b>	4.9	6000	50.0	32.3	17.7	0.55
$[(\equiv\text{SiO})\text{WO}(\text{CHtBu})(\text{dAdPO})]$ , <b>3</b>	7.6	3000	50.0	26.2	23.8	0.91

<sup>a</sup>TOF is expressed in mol of propylene transformed/mol of active W/min. <sup>b</sup>TON is expressed in mol of propylene transformed/mol of active W. <sup>c</sup>Selectivities are defined as the amount of product over the total amount of products, at the end of the reaction (25 h).

about 1 h), giving a maximal conversion of 20% after 5 h. The same kinetic behavior has also been observed for monopodal-anchored tungsten oxo trisneopentyl precatalyst and can be associated with the formation of a tungsten carbene moiety. Contrary to **2b**, the rather long induction period for **2a** can be explained by the steric hindrance due to the presence of three neosilyl ligands, preventing the initial coordination of propylene to the metal center and thus subsequent alkylidene formation. Clearly, **2a** and **2b** showed high stability under a continuous flow of propylene. Furthermore, no formation of polymeric products was observed (by solid-state NMR) after the end of the test. The calculated TON after 25 h is 18 000 for **2a** (24 000 for **2b**), confirming that the bipodal nature has an impact on the catalytic activity in propylene metathesis. The stability of **2a** and **2b** is similar, as shown by the similarity of their slow deactivation profile. The selectivity, provided in Figure S3, remained constant with time on stream, with equimolar quantities of ethylene and 2-butenes (no other alkene was detected). After the onset of the catalysis, the *trans/cis* 2-butene selectivity kept to a constant value of 1.62 (thermodynamic equilibrium = 2.3), in agreement with that observed in the literature for other d<sup>0</sup> systems;<sup>11</sup> that is, terminal alkenes typically give the *trans*-alkene as the major product at relatively high conversion.<sup>38</sup> Further comparison within the same type of catalysts can be made with  $[(\equiv\text{SiO})\text{WO}(\text{CH}_2\text{CMe}_3)_3]$  (**2c**).<sup>12</sup> In this case, we can directly probe the influence of the alkyl ligand (neopentyl vs neosilyl). As shown in Table 2, even if the TOF at 60 min is higher in the case of **2c**, the cumulated TON after 25 h is significantly higher in the case of the neosilyl derivative **2a** (18 000 vs 6000 for **2a** and **2c**, respectively). We have already observed major differences in reactivity of the W–C bond when considering silica grafting of neopentyl and neosilyl derivatives.<sup>21</sup> This was correlated to electronic factors stemming from the presence of the silicon atom. Thus, the beneficial influence of the neosilyl ancillary ligand in alkene metathesis may also be due to such a subtle but actual electronic effect. As the bipodal neopentyl derivative cannot be obtained, even when using SiO<sub>2-200</sub>,<sup>21</sup> the comparison between  $[(\equiv\text{SiO})_2\text{WO}(\text{CH}_2\text{CMe}_3)_2]$  and  $[(\equiv\text{SiO})_2\text{WO}(\text{CH}_2\text{SiMe}_3)_2]$  cannot be drawn.

As a further example of the precautions to be taken when comparing catalysts from the initial TOF, we studied the catalytic propylene conversion by **2a**, **2b**, and a supported tungsten oxo catalyst bearing a bulky aryloxy ligand, namely,  $[(\equiv\text{SiO})\text{WO}(\text{CHtBu})(\text{dAdPO})]$ , **3** (dAdPO = 2,6-AdPhenoxide)<sup>16</sup> (Table 2, Figure S4). Along this series, we have examples of monopodal vs bipodal species (**2a** and **2b**) and of monopodal species bearing a different spectator ligand (neosilyl in **2a** vs bulky phenoxide in **3**).

Table 2 clearly shows that concluding on the activity of a catalyst based on the initial TOF is strongly misleading.

Although the initial TOF (3.3) for **2a** is lower than that of **3** (7.6), its productivity after 25 h is far higher than that of **3** (TON of 18 000 and 3000, respectively), confirming the fact that **2a** is more active and robust than **3**. Previous DFT calculations predicted that unsymmetrical catalysts with a general formula  $W(=E)(=CHR)(X)(Y)$  ( $X \neq Y$ , E = spectator ligand) are systematically more efficient than symmetrical complexes ( $X = Y$ ) when considering the initial TOF and the steady-state approximation, without taking into account experimentally observed activation and deactivation processes.<sup>18</sup> However, experimental results show that the most active and stable catalyst (when considering the TON after a given, realistic time on stream, thus taking into account the deactivation phenomenon) for propylene metathesis is **2b**, which features a symmetrical, bis-siloxide nature. This would call for further examination of the proposed structure–activity relationship.

## CONCLUSION

The new well-defined precatalyst  $[(\equiv\text{SiO})\text{WO}(\text{CH}_2\text{SiMe}_3)_3]$  (**2a**) was obtained by grafting the molecular  $[\text{WO}(\text{CH}_2\text{SiMe}_3)_3\text{Cl}]$  (**1**) precursor on silica dehydroxylated at 700 °C, as demonstrated by mass balance analysis, elemental analysis, IR, advanced solid-state NMR (1D and 2D <sup>1</sup>H, <sup>13</sup>C, <sup>29</sup>Si, and <sup>17</sup>O), EXAFS, and DFT calculations. Furthermore, the present studies aim at the comparison of precatalysts of the type  $[(\equiv\text{SiO})\text{WO}(\text{CH}_2\text{SiMe}_3)_2(X)]$ , with X = CH<sub>2</sub>SiMe<sub>3</sub> (**2a**), O–Si≡ (**2b**), and O–Ar (Ar = 2,6-Ad-phenoxide, **3**), and  $[(\equiv\text{SiO})\text{WO}(\text{CH}_2\text{CMe}_3)_3]$  (**2c**) in propylene self-metathesis under a continuous flow reactor. Thus, we could probe the impact of (i) the podality ( $[(\equiv\text{SiO})\text{WO}(\text{CH}_2\text{SiMe}_3)_3]$ , **2a**, vs  $[(\equiv\text{SiO})_2\text{WO}(\text{CH}_2\text{SiMe}_3)_2]$ , **2b**), (ii) the ancillary ligand ( $[(\equiv\text{SiO})\text{WO}(\text{CH}_2\text{SiMe}_3)_3]$ , **2a**, vs  $[(\equiv\text{SiO})\text{WO}(\text{CH}_2\text{SiMe}_3)(\text{OAr})]$ , **3**), and (iii) the alkyl moiety nature ( $[(\equiv\text{SiO})\text{WO}(\text{CH}_2\text{SiMe}_3)_3]$ , **2a**, vs  $[(\equiv\text{SiO})\text{WO}(\text{CH}_2\text{CMe}_3)_3]$ , **2c**) within the supported tungsten oxo precatalysts. On the basis of the overall TON, the symmetric bipodal precatalyst **2b** (expressed as  $[W(=E)(=CHR)(X)(Y)]$ , X = Y, E = spectator ligand) showed higher activity in propylene metathesis at 80 °C than the asymmetric monopodal catalysts (expressed as  $[W(=E)(=CHR)(X)(Y)]$ , X ≠ Y, E = spectator ligand; **2a**, **2c**, and **3**). Furthermore, the aryloxy derivative **3** afforded catalytic species less stable than those resulting from the trisneosilyl precursor **2a**, most probably due to deactivation through C–H activation. Finally, a subtle change such as the switch from neosilyl (**2a**) to neopentyl (**2c**) within the trisalkyl precursor has a significant influence on the catalytic performances of the resulting active species. These are the first elements in the establishment of structure–activity relationships within this family of olefin metathesis precatalysts,

and they illustrate how the coordination sphere can influence the catalytic performances of the considered surface organometallic species.

## EXPERIMENTAL SECTION

All experiments were carried out by using standard Schlenk and glovebox techniques. Solvents were purified and dried according to standard procedures.  $C_6D_6$  (SDS) was distilled from NaK and stored in a glovebox.  $[W(\equiv CSiMe_3)(CH_2SiMe_3)_3]$  was synthesized following the literature procedure.  $^{17}O$ -Enriched  $[WO(CH_2SiMe_3)_3Cl]$  was prepared using 90 wt %  $^{17}O$ -labeled water. Propylene (Air Liquide, 99.5%) was dried and deoxygenated before use by passing it through freshly regenerated molecular sieves (3 Å) and R-3-15 catalysts (BASF).  $SiO_{2-(200)}$  and  $SiO_{2-(700)}$  were prepared from Aerosil silica (Degussa, specific area of  $200\text{ m}^2\text{ g}^{-1}$ ), which was dehydroxylated at 200 and 700 °C respectively under high vacuum ( $10^{-5}$  Torr) for 15 h to give a white solid having a specific surface area of  $190\text{ m}^2\text{ g}^{-1}$  and containing 2.3 and  $0.7\text{ OH nm}^{-2}$ , respectively. Elemental analyses were performed at the Pascher Mikroanalytisches Labor at Remagen-Bandorf (Germany). IR spectra were recorded on a Nicolet 6700 FT-IR spectrometer by using a DRIFT cell equipped with  $CaF_2$  windows. The samples were prepared under argon within a glovebox. Typically, 64 scans were accumulated for each spectrum (resolution  $4\text{ cm}^{-1}$ ).

**NMR Characterization.** Solution NMR spectra were recorded on an Avance-300 Bruker spectrometer. All chemical shifts were measured relative to residual  $^1H$  or  $^{13}C$  resonances in the deuterated solvent:  $C_6D_6$ ,  $\delta$  7.15 ppm for  $^1H$ , 128 ppm for  $^{13}C$ .  $^1H$  and  $^{13}C$  solid-state NMR spectra were recorded on Bruker Avance-500 and Bruker Avance-300 spectrometers with a conventional double-resonance 4 mm CP MAS probe. The samples were introduced under argon in a zirconia rotor (4 mm), which was then tightly closed. In all experiments, the rotation frequency was set to 10 kHz unless otherwise specified. Chemical shifts were given with respect to TMS as external reference for  $^1H$  and  $^{13}C$  NMR. The  $^{17}O$  solid-state NMR spectra were acquired on Bruker Avance III 800 ( $^{17}O$ , 108.47 MHz) and 900 ( $^{17}O$ , 122.11 MHz) spectrometers, using a single pulse sequence (pulse excitation of  $2\text{ }\mu\text{s}$  at an RF field strength of 60 kHz) and 3.2 mm diameter rotor. No proton decoupling was applied. The recycle delay was 1 s.

**Preparation and Characterization of  $[WO(CH_2SiMe_3)_3Cl]$  (1).** Two equivalents of  $H_2O$  (81  $\mu\text{L}$ , 4.522 mmol) in 45 mL of THF was added dropwise at  $-78\text{ }^\circ\text{C}$  to a vigorously stirred solution of  $[W(\equiv CSiMe_3)(CH_2SiMe_3)_3]$  (1.2 g, 2.261 mmol) in 50 mL of THF. The temperature was slowly raised to  $-40\text{ }^\circ\text{C}$ , where the solution turned red. After 30 min the solution was then allowed to warm to room temperature. Then 2 equiv of  $Me_3SiCl$  (0.57 mL, 4.522 mmol) was added to the reaction mixture. An immediate color change from reddish-orange to yellow was observed upon addition of  $Me_3SiCl$ . The solvent was then removed under vacuum to leave a pale solid. The crude material was sublimed at  $80\text{ }^\circ\text{C}$  under reduced pressure ( $10^{-5}$  mbar) to yield 0.78 g of pure white product (70% yield):  $^1H$  NMR (ppm,  $C_6D_6$ ):  $\delta$  2.29 (6 H, s,  $CH_2Si(CH_3)_3$ ,  $^2J_{(WH)} = 11.0\text{ Hz}$ ), 0.20 (27 H, s,  $CH_2Si(CH_3)_3$ ,  $^{13}C\{^1H\}$  NMR (ppm,  $C_6D_6$ ):  $\delta$  76.13 [ $CH_2Si(CH_3)_3$ ,  $^1J_{(WC)} = 85.1\text{ Hz}$ ], 1.95 [ $CH_2Si(CH_3)_3$ ].  $^{29}Si$  NMR (ppm,  $C_6D_6$ ):  $\delta$  0.9 [ $CH_2Si(CH_3)_3$ ].

**Preparation and Characterization of  $[WO(CH_2SiMe_3)_3Cl]/SiO_{2-700}$  (2a).** A mixture of finely ground  $[WO(CH_2SiMe_3)_3Cl]$  (175 mg, 0.351 mmol) and  $SiO_{2-700}$  (1 g) was stirred at  $40\text{ }^\circ\text{C}$  (5 h) under dynamic vacuum while all volatile compounds were condensed into a cold trap. Pentane was then added, and the solid was washed five times. The resulting white powder was dried under vacuum ( $10^{-5}$  Torr). Elemental analysis: W 4.54% wt; C 3.42% wt.  $^1H$  MAS NMR (500 MHz):  $\delta$  0.1 and 1.3 ppm.  $^{13}C$  CP MAS NMR (125 MHz):  $\delta$  66.2 and  $-0.5$  ppm.  $^{29}Si$  CP MAS NMR (99 MHz):  $\delta$  1.2 ppm.

**Quantification of HCl Released during Grafting.** The gas phase released during grafting was condensed into an IR cell equipped with  $CaF$  windows. Transmission infrared spectra were recorded on a Nicolet 5700 FT spectrometer, at room temperature. The resolution

was  $1\text{ cm}^{-1}$  with 16 scans. HCl was quantified by comparison of the surface of the absorbance IR bands in the  $2600\text{--}3100\text{ cm}^{-1}$  region of the sample to a calibration curve. For the calibration, known amounts of pure HCl were introduced into the same gas cell.

**Propylene Metathesis.** The assessment of the activity of the catalysts in propylene metathesis was performed in a 1/2 in. stainless steel continuous flow reactor. The catalytic tests were performed at  $80\text{ }^\circ\text{C}$ , with a flow rate of  $20\text{ mL min}^{-1}$  and 55 mg of 2a. The products were analyzed by online GC (HP 6890) equipped with a  $KCl/Al_2O_3$  column and a FID. The conversion and selectivity were calculated from carbon numbers.

**SIMPSON Simulation of  $^{17}O$  MAS NMR Spectra.** All  $^{17}O$  MAS NMR numerical spectra were calculated using the *gcompute* method implemented in the SIMPSON software package.<sup>39</sup> This package described each line shape with nine NMR interaction parameters, which included the isotropic chemical shift ( $\delta_{CS}$ ) defined in eq 1, the quadrupole coupling constant ( $C_Q$ ) and quadrupole asymmetry parameter ( $\eta_Q$ ) defined in eq 2 and eq 3, the CSA ( $\Delta_{CSA}$ ) and chemical shift asymmetry parameter ( $\eta_{CSA}$ ) (in the Haerberlein convention) defined in eq 4 and eq 5, and the Euler angles ( $\alpha$ ,  $\beta$ ,  $\gamma$ ). Here the Euler angles were kept to zero due to the impossibility to assess them with the available experimental data sets. Each numerical simulation was performed with the *zcv4180* crystallite file and 30 gamma angles, with the calculated FID inclusive of all quadrupolar satellites. For the best fit simulations, line broadening of 1000 Hz was applied, along with a Gaussian line broadening of 500 Hz.

$$\delta_{CS} = (\delta_{11} + \delta_{22} + \delta_{33})/3 \quad (1)$$

$$C_Q = e^2qQ/h = eV_{33}Q/h, |V_{33}| \geq |V_{22}| \geq |V_{11}| \quad (2)$$

$$\eta_Q = (V_{11} - V_{22})/V_{33} \quad (1 \geq \eta_Q \geq 0) \quad (3)$$

$$\Delta_{CSA} = \delta_{zz} - (\delta_{xx} + \delta_{yy})/2 = 3\delta/2, |\delta_{zz} - \delta_{CS}| \geq |\delta_{xx} - \delta_{CS}| \geq |\delta_{yy} - \delta_{CS}| \quad (4)$$

with the reduced anisotropy,  $\delta = \delta_{33} - \delta_{CS}$ .

$$\eta_{CSA} = (\delta_{yy} - \delta_{xx})/(\delta_{zz} - \delta_{CS}) \quad (1 \geq \eta_{CSA} \geq 0) \quad (5)$$

**DFT Methodological Details.** All DFT calculations were performed with Gaussian 03.<sup>40</sup> Calculations were carried out at the DFT level of theory using the hybrid functional B3PW91.<sup>41–46</sup> Geometry optimizations were achieved without any symmetry restriction. Calculations of vibrational frequencies were systematically done in order to characterize the nature of stationary points. Gibbs free energies were obtained at  $P = 1\text{ atm}$  and  $T = 298.15\text{ K}$  within the harmonic approximation for frequencies. Stuttgart effective core potentials and their associated basis set were used for silicon and tungsten.<sup>47</sup> The basis sets were augmented by a set of polarization functions ( $\zeta_d = 0.284$  for Si and  $\zeta_f = 0.823$  for W). Hydrogen, chlorine, and oxygen atoms were treated with 6-31G(d,p) double- $\zeta$  basis sets.<sup>48,49</sup> The optimized structures were used for  $^{17}O$  NMR calculations. These calculations were also performed using a higher Duning's correlation consistent basis set cc-PVTZ for the oxygen atoms.<sup>50,51</sup> In all cases, among the various theories available to compute chemical shielding tensors, the gauge including atomic orbital (GIAO) method has been adopted for the numerous advantages it presents.<sup>52–57</sup> The same methodology was used in previous studies involving grafted systems, showing that theoretical results are fairly accurate with respect to experimental values with an error lower than 15% for  $^{29}Si$ ,<sup>31,32</sup> 10% for  $^{31}P$ <sup>58</sup> and  $^{17}O$ ,<sup>13,23,30,35</sup> and 5% for  $^1H$  and  $^{13}C$ .<sup>59</sup> Typically, in order to compare our calculations with experimental values,  $^{17}O$  chemical shielding has been converted to chemical shift using the usual equation  $\delta_{iso} = \sigma_{iso\text{ ref}} - \sigma_{iso\text{ sample}}$  where  $\sigma_{iso\text{ ref}}$  is the isotropic  $^{17}O$  chemical shielding of the liquid water. In a continuation of our previous studies,<sup>13,23,30,35</sup> an internal reference is used for the calibration of the  $\sigma_{iso\text{ ref}}$  value:  $\sigma_{iso\text{ ref}} = 292.2\text{ ppm}$ . The  $^{17}O$  quadrupolar coupling constant  $C_Q$  and the asymmetry parameter  $\eta_Q$  which describes the interaction between the nuclear quadrupolar

moment of the oxygen nuclei and the electric field gradient (EFG) arising at these sites, are calculated from the EFG tensor eigenvalues  $V_{11}$ ,  $V_{22}$ , and  $V_{33}$ .

**EXAFS.** X-ray absorption spectra were acquired at the ESRF, using the Swiss-Norwegian beamline BM01B (proposal # 01-01-905), at room temperature at the tungsten  $L_{III}$  edge, with a double-crystal Si(111) monochromator detuned 70% to reduce the higher harmonics of the beam. The spectra were recorded in the transmission mode between 9.98 and 11.45 keV. The supported W sample was packaged within an argon-filled glovebox in a double airtight sample holder equipped with Kapton windows. The spectra analyzed were the results of four such acquisitions, and no evolution could be observed between the first and last acquisition. The data analyses were performed by standard procedures using in particular the program Athena<sup>60</sup> and the EXAFS fitting program RoundMidnight<sup>61</sup> from the MAX package, using spherical waves. The program FEFF8 was used to calculate theoretical files for phases and amplitudes based on model clusters of atoms.<sup>62</sup> The value of the scale factor,  $S_0^2 = 0.94$ , was determined from the  $k^2$  and  $k^3\chi(k)$  spectra of a reference compound, a sample of  $[WO(CH_2tBu)_3Cl]$  complex diluted in BN and carefully mixed and pressed as a pellet (one oxo at 1.70(1) Å, three carbon atoms at 2.10(1) Å, and one chlorine at 2.43(1) Å in the first coordination sphere, with three carbon atoms at 3.28(3) Å).<sup>13</sup> The refinements were performed by fitting the structural parameters  $N_i$ ,  $R_i$ ,  $\sigma_i$ , and the energy shift,  $\Delta E_0$  (the same for all shells). The fit residue,  $\rho(\%)$ , was calculated by the following formula:

$$\rho = \frac{\sum_k [k^3\chi_{\text{exp}}(k) - K^3\chi_{\text{cal}}(k)]^2}{\sum_k [k^3\chi_{\text{exp}}(k)]^2} \times 100$$

As recommended by the Standards and Criteria Committee of the International XAFS Society, the quality factor,  $(\Delta\chi)^2/\nu$ , where  $\nu$  is the number of degrees of freedom in the signal, was calculated, and its minimization considered in order to control the number of variable parameters in the fits.

## ■ ASSOCIATED CONTENT

### Supporting Information

The Supporting Information is available free of charge on the ACS Publications website at DOI: [10.1021/acs.organomet.6b00220](https://doi.org/10.1021/acs.organomet.6b00220).

Additional details on DFT calculations and catalysis (PDF)

Cartesian coordinates (XYZ)

## ■ AUTHOR INFORMATION

### Corresponding Authors

\*E-mail: [laurent.maron@irsamc.ups-tlse.fr](mailto:laurent.maron@irsamc.ups-tlse.fr).

\*E-mail: [laurent.delevoeye@ensc-lille.fr](mailto:laurent.delevoeye@ensc-lille.fr).

\*E-mail: [mostafa.taoufik@univ-lyon1.fr](mailto:mostafa.taoufik@univ-lyon1.fr).

### Notes

The authors declare no competing financial interest.

## ■ ACKNOWLEDGMENTS

This work was funded by the Agence Nationale de la Recherche (ANR-12-BS07-0021-01, OXOCAT). CNRS, French Ministry of Research and Higher Education, Institut de Chimie de Lyon, Chevreul Institute (FR 2638), Région Nord-Pas de Calais, FEDER, are acknowledged for their supplementary support. Financial support from the TGE RMN THC Fr3050 for conducting the high-field solid-state NMR is gratefully acknowledged. We thank the HPCs CALcule, Midi-Pyrénées (CALMIP-EOS, grant P0833), for the generous allocation of computer time. We would also like to thank Hermann Emerich for his help during the recording of the XAS spectra on the

Swiss-Norwegian beamline, BM01B, at ESRF (proposal # 01-01-905).

## ■ REFERENCES

- (1) Lwin, S.; Wachs, I. E. *ACS Catal.* **2014**, *4*, 2505–2520.
- (2) van Schalkwyk, C.; Spamer, A.; Moodley, D. J.; Dube, T.; Reynhardt, J.; Botha, J. M. *Appl. Catal., A* **2003**, *255*, 121–131.
- (3) Maksasithorn, S.; Praserthdam, P.; Suriye, K.; Devillers, M.; Debecker, D. P. *Appl. Catal., A* **2014**, *488*, 200–207.
- (4) Bhuiyan, T. I.; Arudra, P.; Akhtar, M. N.; Aitani, A. M.; Abudawoud, R. H.; Al-Yami, M. A.; Al-Khattaf, S. S. *Appl. Catal., A* **2013**, *467*, 224–234.
- (5) Debecker, D. P.; Stoyanova, M.; Rodemerck, U.; Colbeau-Justin, F.; Boissere, C.; Chaumonnot, A.; Bonduelle, A.; Sanchez, C. *Appl. Catal., A* **2014**, *470*, 458–466.
- (6) Hu, J. C.; Wang, Y. D.; Chen, L. F.; Richards, R.; Yang, W. M.; Liu, Z. C.; Xu, W. *Microporous Mesoporous Mater.* **2006**, *93*, 158–163.
- (7) Maksasithorn, S.; Debecker, D. P.; Praserthdam, P.; Panpranot, J.; Suriye, K.; Ayudhya, S. K. N. *Chin. J. Catal.* **2014**, *35*, 232–241.
- (8) Wang, Y. D.; Chen, Q. L.; Yang, W. M.; Xie, Z. K.; Xu, X.; Huang, D. *Appl. Catal., A* **2003**, *250*, 25–37.
- (9) Spamer, A.; Dube, T. I.; Moodley, D. J.; van Schalkwyk, C.; Botha, J. M. *Appl. Catal., A* **2003**, *255*, 153–167.
- (10) Grunert, W.; Feldhaus, R.; Anders, K.; Shpiro, E. S.; Minachev, K. M. *J. Catal.* **1989**, *120*, 444–456.
- (11) Popoff, N.; Mazoyer, E.; Pelletier, J.; Gauvin, R. M.; Taoufik, M. *Chem. Soc. Rev.* **2013**, *42*, 9035–9054.
- (12) Mazoyer, E.; Merle, N.; de Mallmann, A.; Basset, J. M.; Berrier, E.; Delevoeye, L.; Paul, J. F.; Nicholas, C. P.; Gauvin, R. M.; Taoufik, M. *Chem. Commun.* **2010**, *46*, 8944–8946.
- (13) Merle, N.; Girard, G.; Popoff, N.; De Mallmann, A.; Bouhouste, Y.; Trebosc, J.; Berrier, E.; Paul, J. F.; Nicholas, C. P.; Del Rosal, I.; Maron, L.; Gauvin, R. M.; Delevoeye, L.; Taoufik, M. *Inorg. Chem.* **2013**, *52*, 10119–10130.
- (14) Solans-Monfort, X.; Coperet, C.; Eisenstein, O. *Organometallics* **2012**, *31*, 6812–6822.
- (15) Hamieh, A.; Chen, Y.; Abdel-Azeim, S.; Abou-hamad, E.; Goh, S.; Samantaray, M.; Dey, R.; Cavallo, L.; Basset, J. M. *ACS Catal.* **2015**, *5*, 2164–2171.
- (16) Conley, M. P.; Forrest, W. P.; Mougél, V.; Coperet, C.; Schrock, R. R. *Angew. Chem., Int. Ed.* **2014**, *53*, 14221–14224.
- (17) Amakawa, K.; Wrabetz, S.; Kroehnert, J.; Tzolova-Mueller, G.; Schloegl, R.; Trunschke, A. *J. Am. Chem. Soc.* **2012**, *134*, 11462–11473.
- (18) Poater, A.; Solans-Monfort, X.; Clot, E.; Coperet, C.; Eisenstein, O. *J. Am. Chem. Soc.* **2007**, *129*, 8207–8216.
- (19) Gauvin, R. M.; Coutelier, O.; Berrier, E.; Mortreux, A.; Delevoeye, L.; Paul, J.-F.; Mamede, A.-S.; Payen, E. *Dalton Trans.* **2007**, 3127–3130.
- (20) Bini, F.; Rosier, C.; Saint-Arroman, R. P.; Neumann, E.; Dablemont, C.; de Mallmann, A.; Lefebvre, F.; Niccolai, G. P.; Basset, J. M.; Crocker, M.; Buijink, J. K. *Organometallics* **2006**, *25*, 3743–3760.
- (21) Scott, S. L.; Fu, A. Q.; MacAdams, L. A. *Inorg. Chim. Acta* **2008**, *361*, 3315–3321.
- (22) Szeto, K. C.; Loges, B.; Merle, N.; Popoff, N.; Quadrelli, A.; Jia, H. P.; Berrier, E.; De Mallmann, A.; Delevoeye, L.; Gauvin, R. M.; Taoufik, M. *Organometallics* **2013**, *32*, 6452–6460.
- (23) Bouhouste, Y.; Grekov, D.; Szeto, K. C.; Merle, N.; De Mallmann, A.; Lefebvre, F.; Raffa, G.; Del Rosal, I.; Maron, L.; Gauvin, R. M.; Delevoeye, L.; Taoufik, M. *ACS Catal.* **2016**, *6*, 1–18.
- (24) Sawant, D. P.; Vinu, A.; Mirajkar, S. P.; Lefebvre, F.; Ariga, K.; Anandan, S.; Mori, T.; Nishimura, C.; Halligudi, S. B. *J. Mol. Catal. A: Chem.* **2007**, *271*, 46–56.
- (25) Feinstein-Jaffe, I.; Gibson, D.; Lippard, S. J.; Schrock, R. R.; Spool, A. *J. Am. Chem. Soc.* **1984**, *106*, 6305–6310.
- (26) Legzdins, P.; Rettig, S. J.; Sanchez, L. *Organometallics* **1985**, *4*, 1470–1471.
- (27) Lehtonen, A.; Sillanpää, R. *Acta Crystallogr., Sect. C: Cryst. Struct. Commun.* **1998**, *54*, 935–937.

- (28) Morton, L. A.; Miao, M.; Callaway, T. M.; Chen, T.; Chen, S.-J.; Tuinman, A. A.; Yu, X.; Lu, Z.; Xue, Z.-L. *Chem. Commun.* **2013**, *49*, 9555–9557.
- (29) Sergienko, V. S.; Kovalenko, Y. V.; Ilyukhin, A. B.; Abramenko, V. L. *Zh. Neorg. Khim.* **1994**, *39*, 1320–1327.
- (30) Bouhoute, Y.; Garron, A.; Grekov, D.; Merle, N.; Szeto, K. C.; De Mallmann, A.; Del Rosal, I.; Maron, L.; Girard, G.; Gauvin, R. M.; Delevoye, L.; Taoufik, M. *ACS Catal.* **2014**, *4*, 4232–4241.
- (31) del Rosal, I.; Gerber, I.; Poteau, R.; Maron, L. *New J. Chem.* **2015**, *39*, 7703–7715.
- (32) del Rosal, I.; Gerber, I. C.; Poteau, R.; Maron, L. *J. Phys. Chem. A* **2010**, *114*, 6322–6330.
- (33) del Rosal, I.; Poteau, R.; Maron, L. *Dalton Trans.* **2011**, *40*, 11228–11240.
- (34) del Rosal, I.; Poteau, R.; Maron, L. *Dalton Trans.* **2011**, *40*, 11211–11227.
- (35) Merle, N.; Trebosc, J.; Baudouin, A.; Del Rosal, I.; Maron, L.; Szeto, K.; Genelot, M.; Mortreux, A.; Taoufik, M.; Delevoye, L.; Gauvin, R. M. *J. Am. Chem. Soc.* **2012**, *134*, 9263–9275.
- (36) Pelletier, J.; Basset, J. M. *Acc. Chem. Res.* **2016**, *49*, 664–677.
- (37) Mougél, V.; Coperet, C. *ACS Catal.* **2015**, *5*, 6436–6439.
- (38) Popoff, N.; Szeto, K. C.; Merle, N.; Espinas, J.; Pelletier, J.; Lefebvre, F.; Thivolle-Cazat, J.; Delevoye, L.; De Mallmann, A.; Gauvin, R. M.; Taoufik, M. *Catal. Today* **2014**, *235*, 41–48.
- (39) Bak, M.; Rasmussen, J. T.; Nielsen, N. C. *J. Magn. Reson.* **2000**, *147*, 296–330.
- (40) Frisch, M. J.; Trucks, G. W.; Schlegel, H. B.; Scuseria, G. E.; Robb, M. A.; Cheeseman, J. R.; Montgomery, J. A., Jr.; V. T.; Kudin, K. N.; Burant, J. C.; Millam, J. M.; Iyengar, S. S.; Tomasi, J.; Barone, V.; Mennucci, B.; Cossi, M.; Scalmani, G.; Rega, N.; Petersson, G. A.; Nakatsuji, H.; Hada, M.; Ehara, M.; Toyota, K.; Fukuda, R.; Hasegawa, J.; Ishida, M.; Nakajima, T.; Honda, Y.; Kitao, O.; Nakai, H.; Klene, M.; Li, X.; Knox, J. E.; Hratchian, H. P.; Cross, J. B.; Bakken, V.; Adamo, C.; Jaramillo, J.; Gomperts, R.; Stratmann, R. E.; Yazyev, O.; Austin, A. J.; Cammi, R.; Pomelli, C.; Ochterski, J. W.; Ayala, P. Y.; Morokuma, K.; Voth, G. A.; Salvador, P.; Dannenberg, J. J.; Zakrzewski, V. G.; Dapprich, S.; Daniels, A. D.; Strain, M. C.; Farkas, O.; Malick, D. K.; Rabuck, A. D.; Raghavachari, K.; Foresman, J. B.; Ortiz, J. V.; Cui, Q.; Baboul, A. G.; Clifford, S.; Cioslowski, J.; Stefanov, B. B.; Liu, G.; Liashenko, A.; Piskorz, P.; Komaromi, I.; Martin, R. L.; Fox, D. J.; Keith, T.; Al-Laham, M. A.; Peng, C. Y.; Nanayakkara, A.; Challacombe, M.; Gill, P. M. W.; Johnson, B.; Chen, W.; Wong, M. W.; Gonzalez, C.; Pople, J. A. *Gaussian03*, Revision B.05; Gaussian Inc.: Wallingford, CT, 2003.
- (41) Burke, K.; Perdew, J. P.; Wang, Y., Derivation of a Generalized Gradient Approximation: the PW91 Density Functional. In *Electronic Density Functional Theory: Recent Progress and New Directions*; Dobson, J. F.; Vignale, G.; Mas, M. P., Eds.; Plenum: New York, 1998.
- (42) Perdew, J. P. Unified Theory of Exchange and Correlation Beyond the Local Density Approximation. In *Electronic Structure of Solids*; Ziesche, P.; Eschrig, H., Eds.; Akademie: Berlin, 1991.
- (43) Perdew, J. P.; Burke, K.; Wang, Y. *Phys. Rev. B: Condens. Matter Mater. Phys.* **1996**, *54*, 16533–16539.
- (44) Perdew, J. P.; Burke, K.; Wang, Y. *Phys. Rev. B: Condens. Matter Mater. Phys.* **1998**, *57*, 14999–14999.
- (45) Perdew, J. P.; Chevary, J. A.; Vosko, S. H.; Jackson, K. A.; Pederson, M. R.; Singh, D. J.; Fiolhais, C. *Phys. Rev. B: Condens. Matter Mater. Phys.* **1992**, *46*, 6671–6687.
- (46) Perdew, J. P.; Chevary, J. A.; Vosko, S. H.; Jackson, K. A.; Pederson, M. R.; Singh, D. J.; Fiolhais, C. *Phys. Rev. B: Condens. Matter Mater. Phys.* **1993**, *48*, 4978–4978.
- (47) Kuchle, W.; Dolg, M.; Stoll, H.; Preuss, H. *Mol. Phys.* **1991**, *74*, 1245–1263.
- (48) Hariharan, P. C.; Pople, J. A. *Theor. Chim. Acta* **1973**, *28*, 213–222.
- (49) Hehre, W. J.; Ditchfie, R.; Pople, J. A. *J. Chem. Phys.* **1972**, *56*, 2257–2261.
- (50) Davidson, E. R. *Chem. Phys. Lett.* **1996**, *260*, 514–518.
- (51) Woon, D. E.; Dunning, T. H. *J. Chem. Phys.* **1993**, *98*, 1358–1371.
- (52) Ditchfield, R. *Mol. Phys.* **1974**, *27*, 789–807.
- (53) Dodds, J. L.; McWeeny, R.; Sadlej, A. J. *Mol. Phys.* **1980**, *41*, 1419–1430.
- (54) Junk, P. C.; Steed, J. W. *J. Organomet. Chem.* **1999**, *587*, 191–194.
- (55) London, F. *J. Phys. Radium* **1937**, *8*, 397–409.
- (56) McWeeny, R. *Phys. Rev.* **1962**, *126*, 1028–1034.
- (57) Wolinski, K.; Hinton, J. F.; Pulay, P. *J. Am. Chem. Soc.* **1990**, *112*, 8251–8260.
- (58) Staub, H.; Del Rosal, I.; Maron, L.; Kleitz, F.; Fontaine, F.-G. *J. Phys. Chem. C* **2012**, *116*, 25919–25927.
- (59) Popoff, N.; Espinas, J.; Pelletier, J.; Macqueron, B.; Szeto, K. C.; Boyron, O.; Boisson, C.; Del Rosal, I.; Maron, L.; De Mallmann, A.; Gauvin, R. M.; Taoufik, M. *Chem. - Eur. J.* **2013**, *19*, 964–973.
- (60) Ravel, B.; Newville, M. *J. Synchrotron Radiat.* **2005**, *12*, 537–541.
- (61) Michalowicz, A.; Moscovici, J.; Muller-Bouvet, D.; Provost, K. *J. Phys. Conf. Series* **2009**, *190*, 012034.
- (62) Ankudinov, A. L.; Ravel, B.; Rehr, J. J.; Conradson, S. D. *Phys. Rev. B: Condens. Matter Mater. Phys.* **1998**, *58*, 7565–7576.